Chapter 7
Elucidating Functional Dynamics by $R_{1\rho}$ and R_2 Relaxation Dispersion NMR Spectroscopy

Erik Walinda and Kenji Sugase

Abstract NMR spectroscopy is the method of choice to measure protein and nucleic acid dynamics on a variety of timescales. Picosecond to nanosecond dynamics can be precisely probed by quantifying R_1 and R_2 relaxation rates and heteronuclear NOE values, whereas residual dipolar couplings (RDCs) are sensitive to motion on a wide range of timescales from submicrosecond to milliseconds. Even slower dynamics can be assessed by hydrogen exchange experiments. In a biochemical context, relaxation dispersion NMR spectroscopy is particularly valuable, because it reports on the biologically important timescale from micro- to milliseconds, encompassing the conformational rearrangements of ligand binding, enzymatic reactions, and base pair transitions. From relaxation dispersion measurements, it is possible to obtain structural, kinetic, and thermodynamic information about energetically excited conformational minor states beyond the ground state structure. Here, we review the two methods of $R_{1\rho}$ and R_2 relaxation dispersion, focusing on recent developments in pulse sequence design and data processing techniques, as well as applications of the methods to resolve protein–protein interactions.

Keywords Protein dynamics · Conformational exchange · Protein–ligand interactions · Transverse relaxation

E. Walinda
Department of Molecular and Cellular Physiology,
Graduate School of Medicine, Kyoto University,
Yoshida Konoe-cho, Sakyo-ku, Kyoto 606-8501, Japan
e-mail: walinda.erik.6e@kyoto-u.ac.jp

K. Sugase (✉)
Department of Molecular Engineering,
Graduate School of Engineering, Kyoto University,
Kyoto-Daigaku Katsura, Nishikyo-ku, Kyoto 615-8510, Japan
e-mail: sugase@moleng.kyoto-u.ac.jp

The Nuclear Magnetic Resonance Society of Japan, *Experimental Approaches of NMR Spectroscopy*, https://doi.org/10.1007/978-981-10-5966-7_7

7.1 Relaxation Dispersion

Accurate function of biomolecules such as proteins, carbohydrates, and nucleic acids is central to all cellular processes. Although the function of many proteins and nucleic acids would seem to be explained by a single static structure, many biomacromolecules such as enzymes are extremely dynamic. This dynamical character means that the proteins in fact sample many conformations to exert their physiological function in solution. The static ground state structure of a protein can be obtained from X-ray crystallography, NMR spectroscopy, or cryo-electron microscopy; however, the dynamics beyond this ground state structure remain hidden. Because these "invisible" transient dynamic conformations cannot be observed directly, specialized methods are needed that can detect the energetically excited minor states in solution.

Relaxation dispersion NMR spectroscopy is the method of choice to detect and quantify such functionally relevant motion in biomolecules on a timescale from microseconds to milliseconds. Indeed, relaxation dispersion has provided unprecedented insight, with an astonishing level of detail, into the mechanisms of protein binding [1, 2], enzymatic activity [3–9], base pair exchange [10, 11], post-translational modifications [12], protein folding [13, 14], protein intermediate structures [15], intrinsically disordered proteins [1, 2, 16, 17], and transcriptional activators [18]. This great degree of detail arises (i) because relaxation dispersion provides site-specific information at atomic resolution; and (ii) because the extracted information has such high diversity. The method allows the extraction of structural (chemical shift difference between the major and minor states, $\Delta\omega$), kinetic (lifetime of the excited states, $1/k_{ex}$), and thermodynamic (relative populations of the states, p_i) information about the excited states. Although none of these parameters is directly measurable, the information can be obtained by quantifying the broadening of NMR resonance lines, which is caused by the conformational exchange process.

Relaxation dispersion can be measured by two main methods: R_2 relaxation dispersion and $R_{1\rho}$ relaxation dispersion. In the R_2 relaxation dispersion experiment, the effective transverse relaxation rate is measured as a function of the delay between two successive refocusing pulses in a Carr–Purcell–Meiboom–Gill (CPMG) pulse sequence [19–21]. In the $R_{1\rho}$ relaxation dispersion experiment, the effective rotating-frame relaxation rate is probed as a function of either the amplitude or the offset of an applied spin-lock radiofrequency (RF) field [22–29]. The relaxation rates resulting from either method can then be plotted as a function of the applied field (Fig. 7.1). In the $R_{1\rho}$ relaxation dispersion experiment, the relaxation rates can also be plotted as a function of the spin-lock offset. In either case, fitting of the data points of the relaxation dispersion profile to a theoretical model enables the relevant structural, kinetic, and thermodynamic parameters to be extracted.

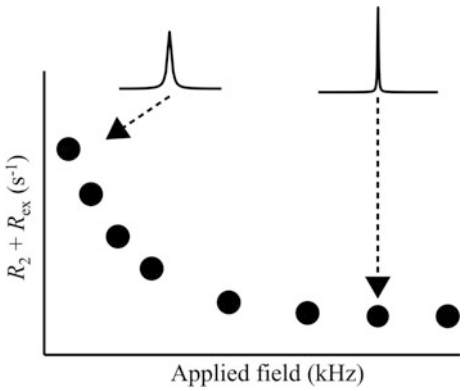

Fig. 7.1 Schematic relaxation dispersion profile. In the presence of chemical exchange (shown), broad signals (large effective R_2) are obtained at weak applied fields, whereas strong fields refocus the magnetization leading to sharp lines (small effective R_2). In the absence of exchange (not shown), the relaxation rates are equal at all applied fields and a flat profile is obtained

In this chapter, we briefly review the two relaxation dispersion methods and then discuss several recent theoretical and practical developments. To this end, we focus on protein–ligand interactions and the automation of relaxation dispersion measurements and processing.

7.2 Accessible Information

The kind of information that can be extracted from relaxation dispersion depends on the exchange regime in question. Assuming the simplest model to describe the exchange between two conformational states A and B in a biomolecule, a two-state exchange model is:

$$\mathrm{A} \underset{k_{\mathrm{BA}}}{\overset{k_{\mathrm{AB}}}{\rightleftarrows}} \mathrm{B}. \tag{7.1}$$

If the exchange between A and B is slow on the chemical shift timescale (slow exchange regime), fitting of the relaxation rates as a function of the applied field strength to a theoretical model yields the chemical shift difference $\Delta\omega$ between the two states, the exchange rate of the process $k_{ex} = k_{AB} + k_{BA}$, and the populations of the major (p_A) and minor state (p_B) [30]. If the exchange process is fast on the chemical shift timescale (fast exchange regime), unfortunately it is not possible to separate p_A, p_B, and $\Delta\omega$ [29, 31]; in this case, only k_{ex}, $R_2{}^0$ (the intrinsic transverse relaxation rate in absence of exchange), and the site of the exchange can be derived and interpreted.

7.3 $R_{1\rho}$ Relaxation Dispersion

7.3.1 General Aspects

Spin-lock-based relaxation dispersion experiments are called $R_{1\rho}$ relaxation dispersion experiments because, during the relaxation block of the pulse sequence, a magnetization decays at the rotating-frame relaxation rate $R_{1\rho}$. In proteins, relaxation of the ^{15}N amide nucleus is most frequently studied [20, 32–34]; however, applications of relaxation dispersion to ^{1}H and ^{13}C nuclei have also been described in the literature [35, 36]. For simplicity, here we focus on the ^{15}N nucleus.

Whether it is possible to resolve a given exchange process by $R_{1\rho}$ relaxation dispersion depends on the exchange rate k_{ex} relative to the applied field strength [29]. That is, the exchange rate k_{ex} should be of the same order as the experimentally applicable effective field amplitudes:

$$\omega_e = \sqrt{\omega_1^2 + \Omega^2}, \tag{7.2}$$

where ω_e is the effective field amplitude (in units of rad s^{-1}). ω_1 and Ω denote the RF field amplitude and the offset of a given resonance from the spin-lock carrier frequency, respectively. In other words, the experimentally applicable field strength directly determines the time window of the dynamical process that can be studied by $R_{1\rho}$ relaxation dispersion. In general, higher effective fields can be used in spin-lock ($R_{1\rho}$ relaxation dispersion) experiments than in CPMG (R_2 relaxation dispersion) experiments; however, spin-lock experiments present other challenges such as accurate field calibration [37], sample heating, and offset effects that are not critical issues with CPMG-type experiments. The spectrometer hardware (amplifier and probe) may impose additional constraints.

When using the ^{15}N amide nucleus as a probe to study the conformational dynamics of a protein, spin-locking fields as high as $\omega_1/2\pi \approx 6$ kHz can be applied [38]. Such strong fields refocus rapidly exchanging magnetization, and thus, very fast chemical exchange processes can be resolved. The spin-lock field can be applied near-resonance ($\Omega \simeq 0$), on-resonance ($\Omega = 0$), or off-resonance ($\Omega \neq 0$). The effective relaxation rate depends on both ω_1 and Ω. Thus, either ω_1 or Ω, or both, can be varied between experiments to obtain spin-lock power (on-resonance $R_{1\rho}$ [28, 39]) or spin-lock offset (off-resonance $R_{1\rho}$ [40, 41])-dependent relaxation dispersion profiles.

Early ^{15}N $R_{1\rho}$ relaxation dispersion experiments were carried out in a relatively conventional manner; in other words, data were obtained as a series of 2D ^{1}H–^{15}N experiments in which a near-resonance spin-lock relaxation building block was included [27, 28, 40, 42]. However, the dependence of the relaxation rate $R_{1\rho}$ on the offset from the spin-lock carrier frequency Ω posed challenges. In particular, because the amide resonances in a protein have different ^{15}N chemical shifts, all resonances experience the effect of the spin lock at different offsets. Thus, these experiments were called “near-resonance” experiments, rather than on-resonance

experiments. The offset dependence imposes the limitation that weak spin-locking fields cannot be used owing to the resulting tilt θ of the effective field toward the z-axis when ω_1 becomes small relative to the offset Ω:

$$\tan\theta = \frac{\omega_1}{\Omega}. \tag{7.3}$$

A highly tilted effective field maximizes the contribution of R_1 and minimizes the contribution of R_2. This is not useful, however, because R_1 does not report on the exchange process in question: Only the transverse relaxation rate R_2 contains an exchange contribution [43]:

$$R_2 = \overline{R_2^0} + R_{\mathrm{ex}}, \tag{7.4}$$

where the line above $R_2{}^0$ indicates that in the case of fast exchange, the relaxation rate will be population-averaged.

In 2005, Kay and coworkers suggested that it would be more beneficial to probe only one of the amide resonances of a protein at a time [25]. An equivalent strategy was also used by Al-Hashimi and coworkers to probe ^{13}C spins in nucleic acids [22]. This strategy eliminates the problem of the differential off-resonance effects of the spins of a protein because only one spin is studied at a time, which is particularly advantageous for off-resonance experiments [25]. Moreover, if desired, the spin lock can be applied completely on-resonance ($\Omega = 0$) in all experiments [44]. To probe a single spin at a time, the pulse sequences utilize Hartmann–Hahn cross-polarization (CP) transfer for selective coherence transfer. Although the number of spectra to be obtained is markedly increased in this scheme, experimental time can be somewhat conserved by recording the experiments as a series of 1D NMR spectra.

When the spin lock is applied on-resonance, accurate spin locking can be achieved even with very weak ω_1 fields. This extends the time window of dynamics that can be studied by $R_{1\rho}$ relaxation dispersion for the study of slow exchange processes, because this window depends on the value of ω_e relative to k_{ex}. Moreover, in this approach, ^{1}H decoupling during the duration of the spin lock is simplified, thereby avoiding potential problems arising from J-coupling and cross-correlation between dipole–dipole interactions and chemical shift anisotropy whenever ^{15}N transverse coherence is present [25].

7.3.2 *Pulse Sequence of the $R_{1\rho}$ Relaxation Dispersion Experiment*

The pulse sequence of a typical $R_{1\rho}$ relaxation dispersion experiment is shown in Fig. 7.2. Equilibrium proton magnetization is excited and transferred to the scalar-coupled amide ^{15}N spin by Hartmann–Hahn cross-polarization [45]. To this

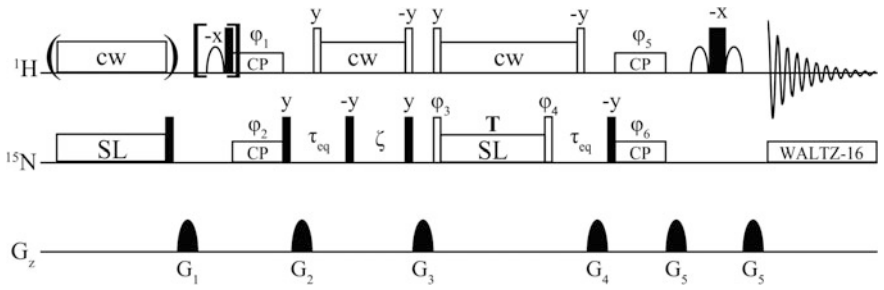

Fig. 7.2 $R_{1\rho}$ relaxation dispersion. Shown is a pulse sequence to probe micro- to millisecond dynamics by ^{15}N $R_{1\rho}$ relaxation dispersion [22, 44]. Pulses are applied with *x* phase, unless noted otherwise in the diagram. The *filled rectangles* denote non-selective 90° pulses. A WATERGATE scheme is used for water suppression [85]. The *open rectangles* represent pulses with variable tip angles as described previously [25]. ^{15}N decoupling during acquisition is achieved by the WALTZ-16 sequence [86]. The block in *square brackets* can be replaced by a selective excitation pulse (E-BURP-1 shape, 5 ms). Phase cycle: $\varphi_1 = 8(y), 8(-y)$; $\varphi_2 = x, -x$; $\varphi_5 = 4(x), 4(-x)$; $\varphi_6 = 2(x), 2(-x)$; $\varphi_{rec} = x, -x, -x, -x, x, x -x, -x, x, x, -x, x, -x, -x, x$; for more details, see ref. [44]. Gradients: G_1 (1 ms, 3 G/cm), G_2 (1 ms, 40 G/cm), G_3 (1 ms, 15 G/cm), G_4 (0.5 ms, 27.5 G/cm), G_5 (1 ms, 10 G/cm). *Abbreviations CP* cross-polarization, *cw* continuous wave irradiation, *SL* spin lock

end, RF fields of matched frequency are applied on both the ^{1}H and the ^{15}N channels. The selectivity of this transfer depends on the amplitude of the matched applied RF fields, which is termed ω_{CP}. In general, it is possible to select a single amide resonance, that is a single cross-peak in a ^{1}H^{15}N–heteronuclear single-quantum coherence (HSQC) spectrum using this technique with very weak matched CP fields, which may be as weak as [46]:

$$\frac{\omega_{CP}}{2\pi} = \frac{\sqrt{3}}{4} J. \tag{7.5}$$

If the resonance in question is sufficiently isolated in the ^{1}H^{15}N–HSQC spectrum, slightly stronger matched CP fields may be applied. By using the program SIMPSON [47], it is possible to simulate the selectivity of this transfer. For example, matched CP fields of $\omega_{CP}/2\pi = 93$ Hz $\approx |J_{HN}|$ cause coherence transfer in an approximate range of ± 100 Hz around the target resonance at a static field of 16.4 T [44]. After CP, the resulting ^{15}N in-phase coherence is stored on the *z*-axis and a *z*-filter is applied to dephase all resonances except the single resonance of interest.

While the coherence of interest is still stored on the *z*-axis, an equilibration time (τ_{eq}) on the order of 5 ms is employed. In some circumstances, the initial population of each state may differ from the expected value if this equilibration period is omitted. Consider a given spin that exchanges between two conformational states A and B, where A is the major state (population $p_A \simeq 0.99$) and B is the minor state (population $p_B \simeq 0.01$). For the given spin, the separation in chemical shift ($\Delta\omega_{AB}$)

between states A and B is relatively large. Thus, when the spin of interest is subjected to selective CP, only the spins of the molecules in which the spin is in state A will feel the effect of selective CP. In other words, only spins in state A transfer their coherence by CP from ^{1}H to ^{15}N. The subsequent z-filter dephases all other resonances, including the spins in state B. Thus, the relative populations of A and B will have been perturbed to $p_A = 1.0$ and $p_B = 0$. The additional equilibration delay τ_{eq} makes sure that, at the beginning of the relaxation period (spin lock), the respective populations p_A and p_B are restored to their appropriate equilibrium values. This is important because the populations appear in the theoretical equations that describe $R_{1\rho}$. Because of this dependence, accurate values of p_A and p_B are critical to ensure a good agreement between theory and experiment. For small values of $\Delta\omega_{AB}$, the influence of τ_{eq} may be limited because spins in state B will be affected by selective CP; however, for $\Delta\omega_{AB}$ values that fall outside the range of the CP coherence transfer profile, the experiment is expected to perform better when a sufficient equilibration delay τ_{eq} is used.

Next, the target magnetization is flipped back to the transverse plane, where the optional delay ζ separates a target on-resonance coherence (^{15}N chemical shift $\Omega = 0$) and a CP-excited nearby unwanted coherence (^{15}N chemical shift $\Omega \neq 0$). If the target coherence is sufficiently isolated in the ^{1}H^{15}N–HSQC spectrum or CP selectivity is sufficient, a value of $\zeta = 0$ may be set: Because ζ is on the order of milliseconds, setting ζ to 0 will maximize sensitivity. The subsequent gradient G_3 dephases the unwanted off-resonance coherences, whereas the target coherence is stored on the z-axis. Whenever ^{15}N transverse coherence is present, ^{1}H decoupling is achieved by applying on-resonance continuous wave fields [25].

As a result, only the single target desired coherence is retained at the beginning of the relaxation period in which the spin lock of variable power and/or offset is applied. After the relaxation block, another equilibration delay is employed and coherence is transferred back from ^{15}N to ^{1}H for detection as a 1D experiment.

The effective rotating-frame relaxation rate is then obtained according to:

$$R_{1\rho} = -\frac{1}{T}\ln\left(\frac{I}{I_0}\right), \tag{7.6}$$

where T is the duration of the spin lock, typically 30–50 ms; I is the peak intensity in an experiment in which a spin lock is applied; and I_0 is a reference intensity from an experiment in which the spin-lock block is omitted (by setting $T = 0$). Note that, because of the dependence of $R_{1\rho}$ on ω_1, the experimentally applied B_1 fields must be rigorously calibrated and their actual values should be measured directly [37].

7.3.3 *Automation of* $R_{1\rho}$ *Relaxation Dispersion Measurements and Data Processing*

Performing the $R_{1\rho}$ relaxation dispersion experiment separately for one site at a time, as described in the previous section, has many advantages because very weak ω_1 fields can be used. However, this approach means that a large number of free-induction decays (FIDs) must be recorded, processed, and integrated before the relaxation rates can be calculated and fitted to a theoretical model. The number of FIDs is $n \times (m + r)$, where n is the number of probed resonances; m is the number of varied parameters, that is, spin-lock power ω_1 or offset Ω (i.e., m is the number of $R_{1\rho}$ relaxation rates (data points) in the final relaxation dispersion profile); and r is the number of reference data recorded. Thus, even for a small protein such as ubiquitin (76 residues; ~72 resolved cross-peaks in the $^{1}H^{15}N$–HSQC spectrum), approximately 1600 ($n = 72$; $m = 20$; $r = 2$) FIDs would have to be recorded, processed, and peak-picked before the $R_{1\rho}$ relaxation rates can be calculated and compared with a theoretical model of the exchange process. It is very likely that many researchers have shied away from this approach to relaxation dispersion owing to its apparently labor-intensive procedure.

It is, however, relatively straightforward to make the acquisition and processing of the data more convenient by considering the following points:

1. Not all amino acids in a protein report on conformational exchange.
2. $R_{1\rho}$ relaxation dispersion-positive residues can be easily identified.
3. Acquisition and processing can be automated.

Based on these three considerations, the acquisition and processing of $R_{1\rho}$ relaxation dispersion data have been recently automated through the development of the *Amaterasu* (automated $R_{1\rho}$ analysis utility) pipeline (Fig. 7.3) [24].

7.3.3.1 Experimental Setup

A dedicated spreadsheet included in the *Amaterasu* package (http://www.moleng.kyoto-u.ac.jp/~moleng_01/amaterasu) calculates all of the acquisition parameters that are required to set up the experiment. The acquisition pulse program is implemented in such a way that the entire dataset, comprising n residues $\times$ $(m + r)$ residue-specific FIDs, is acquired in a single run (i.e., a single acquisition dataset). This type of implementation is termed a "pseudo-2D" experiment and means that only a single experiment needs to be set up at the spectrometer. The acquisition of all residues with all power/offset values is handled entirely by the pulse program.

First, a conventional $^{1}H^{15}N$–HSQC spectrum is acquired. The spectrum is semi-automatically peak picked in a spectrometer acquisition program, such as Bruker TopSpin. The chemical shifts of all resonances of interest are then copied to the *Amaterasu* spreadsheet. At this stage, resonances such as tryptophan side chain

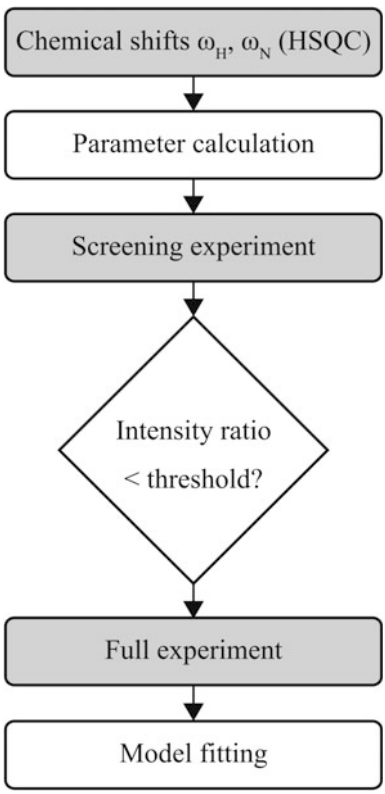

Fig. 7.3 Workflow of *Amaterasu*. *Gray boxes*, experimental steps; *white boxes*, steps automated by the pipeline

peaks can be discarded if desired. After the basic pulse lengths and powers (^{1}H and ^{15}N hard pulses) are entered, the spreadsheet automatically calculates all parameters necessary to perform the $R_{1\rho}$ relaxation dispersion experiment, including CP, spin lock, water-flip back, decoupling pulses, and the optional delay ζ. The chemical shifts ω_H, ω_N, the delay ζ, and the spin-lock power or offset values are passed to the pulse program as simple text files. Once these text files are created, the spreadsheet can be closed.

7.3.3.2 Screening

In almost all known cases, not all residues of a protein will report on conformational exchange on the micro- to millisecond timescale; therefore, it is not recommended that relaxation dispersion profiles are acquired for all residues of a protein, because a great deal of spectrometer time will be spent on acquiring essentially meaningless flat profiles. Instead, an efficient spectroscopist will first identify the dynamic residues of the protein by performing a quick screening experiment in which only two spectra are recorded for all resonances. Each

resonance is probed by a weak and a strong spin-lock field ω_1. For ubiquitin, for example, the ~72 cross-peaks of its $^{1}H^{15}N$–HSQC spectrum would be picked and two spectra would be acquired for each: one with $\omega_1/2\pi \simeq 50$ Hz and one with $\omega_1/2\pi \simeq 3000$ Hz. If the residue in question does not exhibit chemical exchange, the two spectra will show peaks of equal intensity. Conversely, if the resonance does exhibit micro- to millisecond conformational dynamics, a lower peak intensity will be observed in the spectrum corresponding to the weak spin-lock experiment. In summary, a screening experiment will collect only the first and the last data point of a relaxation dispersion profile (Fig. 7.1), with the exception that no reference spectrum is acquired, and thus, the relaxation rate $R_{1\rho}$ is not actually calculated.

If the ratio of these two intensities indicates the presence of chemical exchange, *Amaterasu* will select the resonance for acquisition of a full relaxation dispersion profile. Unpromising resonances can be discarded at this stage to save acquisition time, except for special cases in which a flat profile is particularly desired (e.g., negative control experiments).

7.3.3.3 Processing

The software package *Amaterasu* performs the entire processing procedure from the raw FIDs (in Bruker spectrometer format) to model fitting of the final $R_{1\rho}$ relaxation dispersion profile in a fully automated manner. First, it splits the pseudo-2D dataset into the respective 1D data. Second, it reads all acquisition parameters and, for each FID, conducts apodization, zero filling, 1D Fourier transform (FT), and automatic phase correction. All processing steps are carried out using the Python library nmrglue [48]. For phase correction, the entropy of the spectrum is minimized as described by Chen and coworkers [49]. Third, *Amaterasu* performs peak picking on all spectra. Because the chemical shift of each given resonance is known a priori, the program can easily recognize the correct peak based on the known chemical shift. It is also possible to plot all spectra to check for the presence of artifacts arising from peak overlap or erroneous phases. After all of the peaks are integrated, the resulting peak intensities as a function of ω_1 and/or Ω are passed to the relaxation dispersion data-fitting program GLOVE [50]. The output files of GLOVE will then contain the kinetic and thermodynamic parameters that govern the exchange process, along with the fitted relaxation dispersion profile. For a small protein (~100 amino acids), *Amaterasu* completes its pipeline, from reading the raw FIDs to the final output of the relaxation dispersion profiles, in less than 1 min on a standard desktop PC (e.g., Mac mini, 2015). Examples of relaxation dispersion profiles obtained with *Amaterasu* are shown in Fig. 7.4.

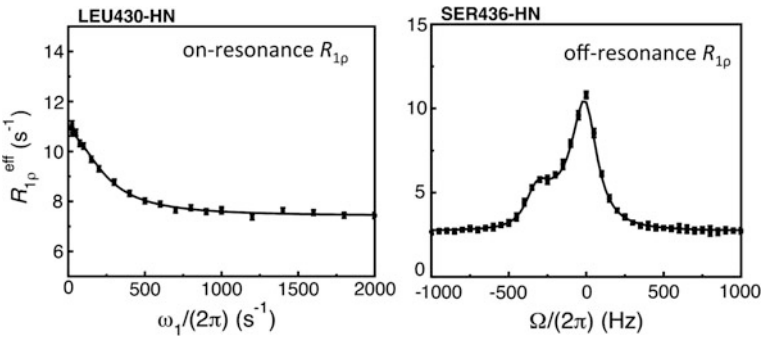

Fig. 7.4 ^{15}N $R_{1\rho}$ relaxation dispersion profiles of amide resonances of the ubiquitin-associated (UBA) domain of the autophagy receptor protein p62 as obtained with *Amaterasu* and GLOVE [24, 50]. *Left*, on-resonance $R_{1\rho}$ relaxation dispersion experiment; *right*, off-resonance $R_{1\rho}$ relaxation dispersion experiment. Reproduced with permission from ref. [24]

7.4 R_2 Relaxation Dispersion

7.4.1 General Aspects

Application of a spin-lock pulse is not the only method to keep a coherence from dephasing during a fixed relaxation delay T. A Carr–Purcell–Meiboom–Gill (CPMG) pulse sequence [19–21] refocuses a given coherence by repetitive execution of the spin-echo sequence $(\tau—180°—2\tau—180°—\tau)_n$. Here, n is an integer and the spacing between the two successive 180° pulses, 2τ, is called τ_{CP}. In general, chemical exchange can be detected by R_2 relaxation dispersion if the exchange rate k_{ex} is of the same order as $1/\tau_{CP}$. As with spin-lock experiments, CPMG experiments may cause sample heating at high values of n, which may also interfere with theoretical treatments of the experiment because the pulse lengths of the refocusing pulses are assumed to be negligible in these models [41, 43].

In principle, the evolution of both in-phase and anti-phase coherences during the CPMG time must be considered. It has been shown, however, that it is beneficial to average the differential contributions of in-phase and anti-phase coherences to R_2 in the experiment by including a relaxation-compensating (RC) element in the pulse sequence (Fig. 7.5). The RC element interconverts in-phase and anti-phase coherences in the middle of the relaxation period, which eliminates any artifacts that may arise from different relaxation rates of in-phase and anti-phase coherences of a spin. For simplicity, the sequence in Fig. 7.5 shows only the pulse sequence during the relaxation time T_{CPMG} including the RC element. In a full sequence, the experiment begins from equilibrium proton magnetization using an INEPT element to obtain the anti-phase ^{15}N coherence $-2H_zN_y$. This coherence is then continuously rephased by the CPMG spin-echo sequence while exhibiting transverse relaxation and imprinting the exchange contribution R_{ex} onto the intrinsic transverse relaxation rate R_2. In the middle of the pulse sequence, the anti-phase coherence $-2H_zN_y$

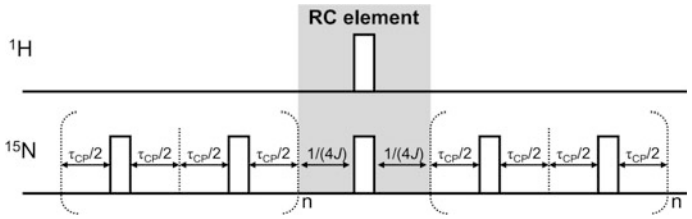

Fig. 7.5 R_2 relaxation dispersion. Shown are pulse sequence elements of a CPMG relaxation dispersion experiment for evolution through the relaxation block of length T_{CPMG}. The sequence starts from an initial coherence described by $-2H_zN_y$, which can be obtained by an INEPT sequence. *Open rectangles* indicate 180° pulses. The relaxation compensation (RC) element interchanges anti-phase to in-phase coherence. J is the amide $^1J_{HN}$-coupling

encounters the RC element and is thus converted to the in-phase coherence N_x; moreover, the RC element suppresses cross-correlation arising from chemical shift anisotropy and dipole–dipole interaction. After passing the RC element, the in-phase coherence N_x relaxes for the remainder of T_{CPMG}, thereby averaging the effect of in-phase and anti-phase coherence relaxation during T_{CPMG}. ^{15}N frequency labeling during t_1 and acquisition during t_2 conclude the experiment.

In the ^{15}N CPMG experiment, problems can arise from $^1J_{HN}$-coupling, offset effects, and pulse imperfections, which can lead to erroneous estimation of the effective transverse relaxation rate R_2^{eff}. These problems can be largely alleviated by applying continuous wave decoupling on the ^{1}H channel during T_{CPMG} [51, 52].

7.4.2 *Quantifying Protein–Ligand Interactions by R_2 Relaxation Dispersion*

Interestingly, relaxation dispersion has not only been used to study the dynamics of a single protein, but it can also probe interactions between a protein and other molecules [31].

When the interaction between a protein and a ligand is in intermediate or slow exchange on the NMR timescale, then the observed chemical shifts do not appear as population averages between the free and bound states in the experiment. In this situation, therefore, other methods that assume fast exchange conditions, such as chemical shift titration or transferred R_1 and R_2 experiments [53–56], are not applicable. For example, for a binding process in the slow exchange regime, the NMR signal of a protein or a ligand does not move during a titration experiment; accordingly, it is not possible to simply obtain a titration curve (chemical shift difference as a function of protein–ligand ratio) to extract the dissociation constant K_D.

In recent years, multiple NMR methods have been developed to study the kinetic rates of slow and intermediate exchange systems. In principle, $R_{1\rho}$ dispersion [28], R_2 dispersion [20, 32, 57, 58], ZZ-exchange [59–61], CEST [62, 63], and DEST

[64] techniques can all be applied to this end; each of these methods has the potential to derive the kinetic rates of interconversion between the states, even though one of the states is not directly measurable because of its low population and a large transverse relaxation rate (due to the additive contribution of R_{ex}).

7.4.2.1 Theory

Consider the interaction between a protein (A) and a ligand (B):

$$\mathrm{A} + \mathrm{B} \underset{k_{off}}{\overset{[\mathrm{B}]k_{on}}{\rightleftarrows}} \mathrm{AB} \tag{7.7}$$

It has been shown that it is possible to determine $[\mathrm{B}]k_{on}$ and k_{off} by relaxation dispersion in an analogous way to determination of the kinetic rates of conformational exchange in a single molecule. Note, however, that [B] is unknown and must be determined. Although it is possible to determine K_D from isothermal titration calorimetry (ITC), to measure k_{off} by NMR, and then to calculate k_{on} from $K_D = k_{off}/k_{on}$ [65], here we discuss the determination of k_{on} and k_{off} without any prior information on K_D by using R_2 relaxation dispersion [1].

If the exchange process—that is, the association–dissociation equilibrium—occurs on the timescale of milliseconds with a comparably large chemical shift change $\Delta\omega$, we can assume that the effective transverse relaxation rate R_2 of the free and the bound resonances will increase by an additional relaxation rate R_{ex}, as described by Eq. 7.4. R_2^{eff} can be obtained from the R_2 relaxation dispersion experiment, thereby allowing extraction of the rate k_{ex} of the association–dissociation process. In addition, structural information in form of the chemical shift difference $\Delta\omega$ between the free and bound states can be obtained. R_2^{eff} can be accurately described by numerical solution of the Bloch–McConnell equations [66, 67]. Alternatively, we can assume a simple two-state exchange model and describe R_2^{eff} as follows [68]:

$$\begin{aligned}
R_2^{\mathrm{eff}} &= R_2^0 + \tfrac{1}{2}\left\{k_{ex} - \tfrac{1}{\tau_{cp}}\cosh^{-1}\left[D_+\cosh\left(\eta_+\right) - D_-\cos(\eta_-)\right]\right\} \\
D_\pm &= \tfrac{1}{2}\left[\pm 1 + \frac{\Psi + 2\Delta\omega^2}{\sqrt{\Psi^2 + \xi^2}}\right] \\
\eta_\pm &= \tau_{cp}\sqrt{\tfrac{1}{2}\left(\pm\Psi + \sqrt{\Psi^2 + \xi^2}\right)} \\
\Psi &= k_{ex}^2 - \Delta\omega^2 \\
\xi &= 2\Delta\omega([\mathrm{B}]k_{on} - k_{off}) \\
k_{ex} &= [\mathrm{B}]k_{on} + k_{off},
\end{aligned} \tag{7.8}$$

where R_2^0 is the intrinsic relaxation rate in the absence of exchange and is assumed to be identical for the free and bound states; and τ_{CP} is the delay between two successive 180° pulses in the CPMG pulse train. τ_{CP} is thus a known, preset

parameter when the experiment is performed. If the interaction between protein and ligand is in the intermediate or slow exchange regime, it is possible to separate the parameter k_{ex} into $[B]k_{on}$ and k_{off}.

In general, the concentration of unbound ligand—namely, the concentration of free B—is described by:

$$[B] = \frac{1}{2}\left\{-K_D - [A]_0 + [B]_0 + \sqrt{\left(K_D + [A]_0 - [B]_0\right)^2 + 4[B]_0 K_D}\right\}, \quad (7.9)$$

where $[A]_0$ and $[B]_0$ are the total concentrations of A and B, respectively. To separate $[B]k_{on}$ in order to calculate k_{on}, we notice that [B] depends on $[A]_0$ and $[B]_0$. As a result, multiple samples with varying total amounts of $[A]_0$ and/or $[B]_0$ can be prepared, and global fits of the R_2 relaxation dispersion profiles can be performed for the various samples. In most cases, it is wise to keep one of the concentrations constant, ideally the concentration $[A]_0$ of the isotope-labeled protein, to obtain relaxation dispersion profiles with similar sensitivity from different measurements. Thus, it is most feasible to vary the total concentration of the unlabeled ligand $[B]_0$. As described in detail in ref. [31], it is necessary to include the total concentrations $[A]_0$ and $[B]_0$ as variable fitting parameters in the fitting procedure under realistic experimental conditions; otherwise, a 5% mismatch of the concentration can lead to a twofold error in the final K_D value. Moreover, the NMR samples for these experiments must be prepared with extreme care—preferably by dilution from single respective concentrated stock solutions—to obtain accurate concentration ratios. Taken together, relaxation dispersion is measured for multiple samples with multiple concentration ratios using a modified version of Eq. 7.9, in which the parameter a is introduced as follows:

$$[B] = \frac{1}{2}\left\{-K_D - [A]_0 + a[B]_0 + \sqrt{\left(K_D + [A]_0 - a[B]_0\right)^2 + 4a[B]_0 K_D}\right\}. \quad (7.10)$$

7.4.2.2 Example 1: Interaction Between the pKID Domain of CREB and the KIX Domain of CBP/p300

The method to obtain K_D by R_2 relaxation dispersion was originally applied to study the phosphorylated kinase-inducible domain (pKID), an intrinsically disordered protein that forms part of the transcription factor CREB. pKID binds to the KIX domain of CBP/p300 [1]. To study the affinity of the two proteins, a [^{15}N]-labeled sample of pKID was prepared and relaxation dispersion profiles were obtained for samples with concentration ratios (KIX/pKID) of 0.95, 1.00, 1.05, and 1.10 at two distinct static magnetic fields of 500 and 800 MHz (Fig. 7.6).

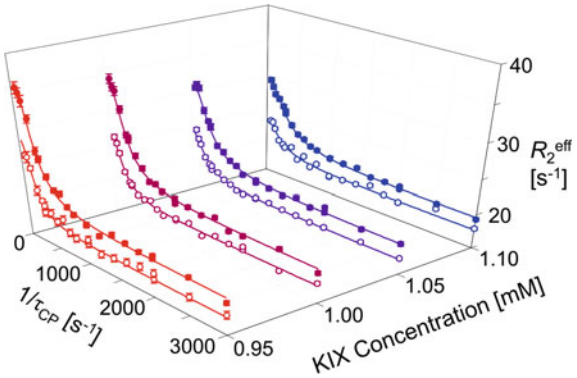

Fig. 7.6 Protein–ligand ratio-dependent R_2 relaxation dispersion profiles. The relaxation dispersion profiles were obtained at 800 MHz (*filled circles*) and 500 MHz (*open circles*). The data (reproduced with permission from [1]) show Arg^{124} of 1 mM pKID in the presence of 0.95, 1.00, 1.05, and 1.10 mM KIX. A global fit of the relaxation dispersion data provided the values of k_{on}, k_{off}, k_1, k_{-1}, and K_D, as well as chemical shift differences between the distinct states

The induced fit model was used to fit all relaxation dispersion data (4 concentration ratios, 2 B_0 values) as follows:

$$\mathrm{A} + \mathrm{B} \underset{k_{off}}{\overset{[\mathrm{B}]k_{on}}{\rightleftarrows}} \underline{\mathrm{A{:}B}} \underset{k_{-1}}{\overset{k_1}{\rightleftarrows}} \mathrm{A{:}B}, \tag{7.11}$$

where the underline indicates that the conformation of the state $\underline{\mathrm{A{:}B}}$ is different from the final bound state A:B. For each residue, the chemical shift differences were defined as global parameters. The folding (k_1) and unfolding (k_{-1}) rates were considered as global parameters for all residues falling within the same cluster, that is, residues that are in close proximity in the same secondary structure element and thus presumably fold/unfold in a cooperative manner. As a result, it was possible to obtain site-specific K_D values for the binding of pKID to KIX. Strikingly, the mean K_D value obtained from the site-specific analysis showed excellent agreement with the global, macroscopic dissociation constant obtained by ITC [69]. Based on the relaxation dispersion data combined with chemical shift titrations, it was concluded that pKID engages with KIX, while it is unfolded through the formation of non-specific encounter complexes; upon KIX binding, pKID adopts a partially folded intermediate, which subsequently evolves toward a fully folded bound state. In other words, this model consists of four distinct states: free pKID, a non-specific encounter complex, a bound-folding intermediate, and the final bound-folded state. Note that this model assumes that the exchange between the free state and the encounter complex is too fast to be traceable by R_2 relaxation dispersion. In summary, relaxation dispersion deciphered the coupled folding and binding mechanism of an intrinsically disordered protein.

7.4.2.3 Example 2: Interaction Between the Transactivation Domain of c-Myb and KIX

The transactivation domain of c-Myb, a transcription factor, also binds the KIX domain. Similar to pKID, the transactivation domain of c-Myb is an intrinsically disordered protein [16]. Again, the mechanism of binding has been resolved in great molecular detail by R_2 relaxation dispersion. In essence, it was deduced that the N-terminal region of c-Myb binds to KIX while already in a principally folded conformation. Conversely, the C-terminal region of c-Myb folds after binding to KIX, and again this binding is explained by an induced fit mechanism.

7.5 Fitting of the Relaxation Rates to a Theoretical Model

The theoretical model used for fitting depends on the exchange regime and the number of exchange sites. A vast amount of work has been done in the development of analytical equations to describe relaxation dispersion (Table 7.1). These equations can be used to fit the experimental relaxation dispersion profiles. Fitting can be performed by implementing a selected equation in commercial or free packages such as Mathematica, MatLab, SciLab, or similar software. Alternatively, a relaxation dispersion-dedicated free software package such as GLOVE (http://www.scripps.edu/wright/?page_id=17) can be used. In the following, we illustrate both theoretical and practical aspects of fitting of relaxation dispersion data by GLOVE.

7.5.1 Least-Squares Fitting in GLOVE

GLOVE is a dedicated relaxation dispersion data-fitting software, although it also supports several other NMR experiments such as R_1, R_2, and CLEANEX-PM [70].

Table 7.1 Reports of analytical equations to approximate relaxation dispersion

Method	Exchange process	Reference
$R_{1\rho}$	2-Site fast exchange	[87]
$R_{1\rho}$	2-Site fast exchange	[88]
$R_{1\rho}$	2-Site exchange	[89]
$R_{1\rho}$	2-Site exchange	[90]
$R_{1\rho}$	2-Site exchange	[91]
$R_{1\rho}$	2-Site exchange	[26]
$R_{1\rho}$	*N*-Site exchange	[92]
R_2	2-Site fast exchange	[93]
R_2	2-Site exchange	[94]
R_2	2-Site exchange	[87]
R_2	2-Site exchange	[68]
R_2	2-Site exchange	[95]

It solves nonlinear least square problems by using the algorithm of Levenberg–Marquardt. GLOVE is written in C++, which assures rapid fitting of the data. To fit the relaxation dispersion profiles, the GLOVE software attempts to minimize the statistical variable χ^2 in an iterative manner. χ^2 is given as a function of the experimental and calculated effective R_2 rates:

$$\chi^2 = \sum_{i=1}^{N} \left(\frac{R_2^{i,\mathrm{exp}} - R_2^{i,\mathrm{calc}}}{\sigma^i} \right)^2 . \tag{7.12}$$

where the variables ${R_2}^{i,\mathrm{exp}}$ and ${R_2}^{i,\mathrm{calc}}$ denote the experimental and calculated values of ${R_2}^{\mathrm{eff}}$, respectively; and the parameter σ^i represents the experimental error.

To minimize the function iteratively, initial parameters must be provided. In GLOVE, there are five distinct methods to provide the initial parameters. Importantly, it is possible to run multiple methods or to repeat the same method. The program stores the parameter set corresponding to the lowest obtained value of χ^2 and replaces this set if a better fit (a lower value of χ^2) is found.

The method named *ONE* is a minimization routine that starts from the lowest limit or an optionally specified value. As soon as the minimization routine finds a local minimum, the fitting process stops. *ONEEX* is equivalent to *ONE*, with the exception that the fitting process does not stop until both global and local parameters (optimized separately) have converged into local minima. When global fitting of parameters is desired, it is advisable to use *ONEEX* even though the fit converges more slowly. The methods *GRID*, *RANDOM,* and *MCMIN* stop when they reach the same condition as described for *ONE*; however, they explore the parameter space much more rapidly at the earlier stages of the fitting procedure.

As indicated by its name, *GRID* represents a grid search. Initially, the global parameters are fixed (to a given grid point) and the local parameters of each dataset are varied using a grid search algorithm. Next, the fix on the global parameters is removed, and then, all parameters including global parameters are optimized. The procedure is iterated to explore all grid points of the parameter space of the global parameters.

Lastly, the methods *RANDOM* and *MCMIN* represent a random search and minimization by a Monte Carlo algorithm, respectively. *RANDOM* uses a random number generator to choose a random initial value from a range of parameters, and χ^2 is subsequently minimized by other iterative methods as specified by the user. Thus, *RANDOM* can be used to quickly find good starting values to determine the global minimum from the entire range of specified parameters. Conversely, *MCMIN* achieves a more accurate determination of the global minimum after initial establishment of the fit parameter set provided by *RANDOM* and other methods. This Monte Carlo implementation in GLOVE is described in detail in the next section.

7.5.2 Monte Carlo Minimization Algorithm in GLOVE

Monte Carlo minimization is a popular method in molecular simulations. For example, it has been used to find the global energy minimum during the folding of a peptide structure by randomly varying the dihedral angles in order to overcome large energy barriers [71]. In a protein-folding context, the Metropolis criterion is used to compare the newly energy-minimized structure with a previous conformation [72, 73]. In the minimization context of GLOVE, the initial parameter values are the currently available best-fit parameters to which positive or negative random numbers, which follow a Gaussian distribution, are added. This enables the parameter set to overcome the barriers of a local minimum. The newly obtained parameter set can then be minimized by using conventional least-squares methods as described above. If the new χ^2 is smaller than the previous value, the Monte Carlo step is accepted.

Monte Carlo minimization (*MCMIN*) runs until no better parameter set is found for a total number of iterations as specified by the user; in general, this number is higher than 5. Moreover, if a lower value of χ^2 is obtained, the iteration counter is reset to 0. The magnitude of the Monte Carlo trial steps can be controlled by the user by specifying a scaling factor in the input file to GLOVE. For efficient minimization of χ^2, it is important to choose this factor judiciously. In particular, a too small scaling factor would not overcome the barriers of a local minimum efficiently. Conversely, if the scaling factor is too large, resulting in a large Monte Carlo step, the new set of parameters may be completely different from the current best parameter set, which may lead to a marked increase in the value of χ^2. An efficient protocol to determine the global minimum most accurately and rapidly is therefore to run *MCMIN* multiple times with successively smaller scaling factors. Because the fitting parameters are far from the best-fit solution at the early stages of fitting, the *MCMIN* scaling factor should be set to a comparably large value. The parameters can be varied very finely by using a small scaling factor in the final stages of the fitting in order to determine the global minimum most accurately.

7.5.3 Two-State Exchange

For simplicity, we describe the most common model used to fit relaxation dispersion data; however, many additional published equations, including two- and three-state exchanges, are available within GLOVE. A relaxation dispersion profile, which reports on a two-state exchange process (Eq. 7.1), is described by the equation of Carver and Richards [68] for all exchange regimes under realistic

experimental conditions. The Carver and Richards equation calculates the effective transverse relaxation constant ${R_2}^{\text{eff}}$ as:

$$
\begin{aligned}
R_2^{\text{eff}} &= \frac{1}{2}\left\{R_{2\text{A}}^0 + R_{2\text{B}}^0 + k_{\text{AB}} + k_{\text{BA}} - \frac{1}{\tau_{\text{CP}}}\cosh^{-1}\left[D_+\cosh\left(\eta_+\right) - D_-\cos(\eta_-)\right]\right\} \\
D_\pm &= \frac{1}{2}\left[\pm 1 + \frac{\Psi + 2\Delta\omega^2}{\sqrt{\Psi^2 + \xi^2}}\right] \\
\eta_\pm &= \tau_{\text{CP}}\sqrt{\frac{1}{2}\left(\pm\Psi + \sqrt{\Psi^2 + \xi^2}\right)} \\
\Psi &= \left(R_{2\text{A}}^0 - R_{2\text{B}}^0 + k_{\text{AB}} - k_{\text{BA}}\right)^2 - \Delta\omega^2 + 4k_{\text{AB}}k_{\text{BA}} \\
\xi &= 2\Delta\omega\left(R_{2\text{A}}^0 - R_{2\text{B}}^0 + k_{\text{AB}} - k_{\text{BA}}\right).
\end{aligned}
\tag{7.13}
$$

Equation 7.13 resembles Eq. 7.8 but has a more general nature. In Eq. 7.13, $\Delta\omega$ denotes the difference in chemical shift between the states A and B and has the units rad s^{-1}; and ${R_{2\text{A}}}^0$ and ${R_{2\text{B}}}^0$ are the transverse relaxation rates of the respective states A and B. Note that Eq. 7.13 considers that these values differ: In principle, the intrinsic transverse relaxation rates may be different; however, in practice, they are usually assumed to be the same. Thus,

$$
{R_2}^0 = {R_{2\text{A}}}^0 = {R_{2\text{B}}}^0. \tag{7.14}
$$

Importantly, this assumption does not have a large effect on the analysis of the exchange process in the case that the rate of the exchange is larger than the difference between ${R_{2\text{A}}}^0$ and ${R_{2\text{B}}}^0$ (i.e., if $k_{\text{ex}} \gg |{R_{2\text{A}}}^0 - {R_{2\text{B}}}^0|$). Moreover, we reduce the parameter space by defining k_{ex} as the sum of the reaction rates of the forward and backward reaction. Thus,

$$
k_{\text{ex}} = k_{\text{AB}} + k_{\text{BA}}. \tag{7.15}
$$

In addition, the product of $p_{\text{A}} \times p_{\text{B}}$ is treated as a single fitting parameter $a = p_{\text{A}}p_{\text{B}}$. After fitting, p_{B} (the population of the minor state) can then be calculated as:

$$
p_{\text{B}} = \frac{\sqrt{1 - 4a}}{2}. \tag{7.16}
$$

This further enhances the efficiency and stability of the calculation. In summary, the Carver and Richards equation [68] is implemented in GLOVE as:

$$
\begin{aligned}
R_2^{\text{eff}} &= R_2^0 + \frac{1}{2}\left\{k_{\text{ex}} - \frac{1}{\tau_{\text{CP}}}\cosh^{-1}\left[D_+\cosh\left(\eta_+\right) - D_-\cos(\eta_-)\right]\right\} \\
D_\pm &= \frac{1}{2}\left[\pm 1 + \frac{\Psi + 2\Delta\omega^2}{\sqrt{\Psi^2 + \xi^2}}\right] \\
\eta_\pm &= \tau_{\text{CP}}\sqrt{\frac{1}{2}\left(\pm\Psi + \sqrt{\Psi^2 + \xi^2}\right)} \\
\Psi &= k_{\text{ex}}^2 - \Delta\omega^2 \\
\xi &= 2\Delta\omega k_{\text{ex}}\sqrt{1 - 4p_{\text{A}}p_{\text{B}}}.
\end{aligned}
\tag{7.17}
$$

Note that GLOVE calculates the partial derivatives of $R_2{}^{\text{eff}}$ (required by the least-squares minimization algorithm) with respect to the fitting parameters analytically instead of numerically, which helps to speed up the calculation.

7.5.4 *Workflow for Processing Relaxation Dispersion Data in GLOVE*

In this section, a practical approach to processing relaxation dispersion data using the software package GLOVE is presented. First, the relaxation dispersion spectra are measured. In the case of $R_{1\rho}$ relaxation dispersion data, *Amaterasu* can be used, which will automatically pass the relaxation rates and spin-lock powers to GLOVE.

In the case of R_2 relaxation dispersion data, additional steps are necessary. Initially, all spectra are processed by exactly the same processing parameters, including the functions for solvent suppression, apodization, Fourier transform, zero- and first-order phase correction, and baseline correction. It is advisable to use a low order for the baseline correction function in order not to perturb the intensities of relatively small signals. It is not feasible to apply linear prediction because it may interfere with quantitative analysis of the NMR data. However, it is possible to reduce the acquisition time of relaxation dispersion datasets by nonlinear sampling methods [74]. Next, it is necessary to obtain the integrated peak intensities to calculate the effective transverse relaxation rates. This is done by using the tool *pkfit*, which is included in the GLOVE package. The experimental error in the peak intensity is calculated from the standard deviation of the amplitudes of the noise in each spectrum and the deviation between peak intensities in duplicated data. Thus, after running *pkfit*, the output file contains the static magnetic field B_0 (MHz), the relaxation time T_{CPMG} (s), and the peak intensities of all resonances as a function of $1/\tau_{\text{CP}}$ (s^{-1}). The delay τ_{CP} in the pulse sequence is the time between two 180° pulses of the CPMG pulse train. Note that some groups use a different notation by defining τ_{CPMG} as half the delay between two 180° pulses; in this case, the relaxation rates are plotted as a function of $\nu_{\text{CPMG}} = 1/(4\tau_{\text{CPMG}})$ instead of $1/\tau_{\text{CP}}$.

Although the horizontal axis differs in the two representations, it is straightforward to convert ν_{CPMG} to $1/\tau_{CP}$ according to:

$$1/\tau_{CP} = 2\nu_{CPMG}. \tag{7.18}$$

In complete analogy to Eq. 7.6, the effective R_2^{eff} relaxation rates are then calculated according to:

$$R_2^{eff}(\tau_{CP}) = -\frac{1}{T_{CPMG}} \ln\left(\frac{I(\tau_{CP})}{I_0}\right), \tag{7.19}$$

where $I(\tau_{CP})$ is the peak intensity in the spectrum corresponding to a particular value of τ_{CP}; and I_0 is the intensity in a reference spectrum in which the relaxation block is omitted (by setting $T_{CPMG} = 0$). This calculation is carried out by the tool *cpmg2glove* in the GLOVE package. Moreover, the experimental error in R_2^{eff} is calculated from the spectral RMSD noise according to [75]:

$$\sigma^i = \frac{\varepsilon_I}{I(\tau_{CP}) \times T_{CPMG}}, \tag{7.20}$$

where ε_I is the RMSD noise of the spectrum. The output of the tool *cpmg2glove* is the input file for GLOVE and contains all data necessary to perform curve fitting of the relaxation dispersion profile. The file may contain only one measurement or multiple different measurements (e.g., under different values of B_0, temperatures or ligand concentrations).

After fitting of the $R_{1\rho}$ or R_2 relaxation dispersion data, GLOVE writes an output file containing a summary of the results and plots of the fitted relaxation dispersion profile in the format Xmgr or Grace. An Xmgr file for each resonance of the dataset is created, but it is possible to combine all of these plots in a single PDF file for convenience. This is achieved by the tool *mplot*, which is included in the GLOVE package. During the fitting process, GLOVE will write the reduced value of χ^2, which is χ^2 divided by the number of degrees of freedom of the fitting model, to the standard output (typically, the console), enabling the user to monitor the convergence of the fit in real time. Uncertainties in the resulting fitting parameters can be calculated by standard deviation, Monte Carlo, and/or jackknife methods [76, 77].

7.5.5 *Examples of Relaxation Dispersion Curve Fitting by GLOVE*

Here, we illustrate curve fitting of relaxation dispersion data by fitting the R_2 relaxation dispersion profiles of KIX. In total, 110 R_2 relaxation dispersion profiles (55 resonances; 2 values of B_0) were subjected to analysis. KIX exhibits a two-state exchange between its native and a non-native conformation [78]. The relaxation

dispersion profiles were obtained at two distinct magnetic fields on a Bruker DRX600 and a Bruker DMX750 spectrometer at a temperature of 25 °C using a [^{15}N]-labeled sample of KIX (concentration: 0.5 mM) [74]. Spectra were acquired for τ_{CP} values of 10, 5, 3.33, 2.5, 2.0, 1.66, 1.43, 1.25, 1.0, 0.83, 0.71, 0.63, 0.55, 0.5, 0.4, and 0.33 ms at a relaxation time, T_{CPMG}, of 40 ms.

The performance of GLOVE was evaluated on an Apple iMac (Intel Core i7 dual core, 3.4 GHz) with the GLOVE executable file compiled by using the Intel C++ compiler [50]. The speed and accuracy of the fit were evaluated by using the directives *ONE*, *ONEEX*, and *GRID*. In addition, the combinations *GRID* + *ONEEX*, *RANDOM* + *ONEEX*, *MCMIN* + *ONEEX*, and *RANDOM* + *MCMIN* + *ONEEX* were tested. A combined workflow of *RANDOM* + *MCMIN* + *ONEEX* was found to yield the best results [50].

The relaxation dispersion profiles of KIX were subjected to a global fit using the Carver and Richards equation [68]. The exchange rate k_{ex} and the product of the populations $p_A p_B$ were specified as global parameters. The possible range of the parameters was specified as [100–2500] for $\Delta\omega$, [5–4000] for k_{ex}, and [0.005–0.09] for the product $p_A p_B$. The initial parameter value of $R_2{}^0$ was taken from the lowest value of $R_2{}^{eff}$ (the right-most data point in the relaxation dispersion profile). For the minimization routines *ONE*, *ONEEX,* and *MCMIN*, the calculation starts from the lower limits of the parameter range. In the evaluation study, grid sizes from 2 to 20 were evaluated for the method *GRID* for the parameters $\Delta\omega$, k_{ex}, $p_A p_B$ [50]. In *MCMIN*, the scaling factor was sequentially reduced from 0.1 to a final value of 0.001. Note that, because *RANDOM* and *MCMIN* rely on random number generators, they provide a different result at each execution. Thus, methods relying only on *RANDOM* on *MCMIN* alone were repeated 10 times to evaluate the average and standard deviation of each fit.

The 110 relaxation dispersion profiles of KIX were subjected to a global fit, where the overall lowest value of χ^2, reached by many methods, was 1.45047, indicating that it represents the global minimum. At this value of χ^2, the global parameters of the exchange rate k_{ex} converged to $600 \pm 5\ s^{-1}$. Moreover, the product of $p_A p_B$ converged to 0.0343 ± 0.0002. Examples of the corresponding relaxation dispersion profiles are shown in Fig. 7.7. Note that these plots were obtained directly from GLOVE and no further adjustment of the image to obtain publication quality was necessary.

The global minimum was not found by *ONE*, which means that relaxation dispersion profile fitting has the intrinsic problem of becoming trapped in local minima (Table 7.2). Thus, good initial values, or alternatively multiple fits starting from different initial parameters, are necessary to find the global minimum. *ONEEX* found a smaller χ^2 value; however, it did not locate the global minimum either. The *GRID* method with a grid size of 11 resulted in a χ^2 value of 1.45056, which is very near to the global minimum. Moreover, when *ONEEX* was followed by *GRID*, the global minimum was always found. Thus, *ONEEX* is very useful at the last stages of the fit to converge to the global minimum. Importantly, fitting strategies that used only *RANDOM* or *MCMIN* alone did not find the global minimum. Conversely,

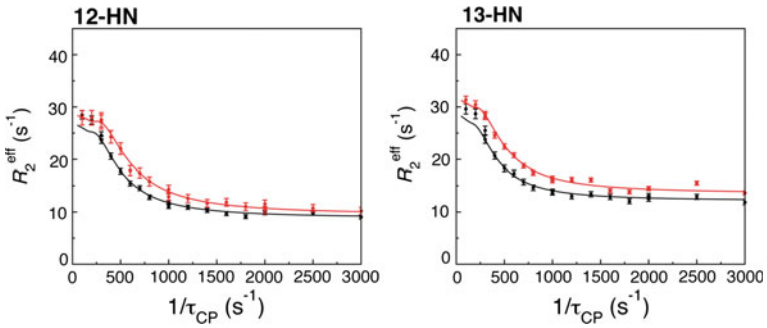

Fig. 7.7 Relaxation dispersion profiles for KIX as fitted by GLOVE. The *best-fit curves* are shown for a dataset collected at a ^{15}N frequency of 60.83 MHz (*black line*) and 76.01 MHz (*red line*), respectively. Residue numbers are indicated at the *top* (–HN)

Table 7.2 Relaxation dispersion curve-fitting methods in GLOVE

Method	Reduced χ^2 value[a]
ONE	14.9719
ONEEX	9.82986
RANDOM + ONEEX	2.06638 → 1.45047
RANDOM + MCMIN + ONEEX	3.70891 → 1.45052 → 1.45047
MCMIN + ONEEX	9.54153 → 8.93963

Additional details are given in Ref. [50]
[a]The initial reduced χ^2 was 88.7611

when applying *ONEEX* after *RANDOM*, the global minimum was always found. Likewise, the combination *RANDOM* + *MCMIN* + *ONEEX* always found the global minimum and was computationally faster than other methods.

7.6 Outlook

Without a doubt, both $R_{1\rho}$ and R_2 relaxation dispersion will continue to contribute to the elucidation of a myriad of functionally important dynamical processes in the life of biomolecules such as proteins and nucleic acids. If sufficiently accurate relaxation dispersion profiles are obtained, standard desktop computers are now fast enough to solve Bloch–McConnell equations numerically without relying on approximate methods (Table 7.1). Application of relaxation dispersion to larger molecules

remains challenging because of signal overlap and other complications; however, methods are continuously being developed to tackle these challenges [79–82].

The great wealth of information provided by relaxation dispersion sometimes overshadows the most important question in this context. What *is* the excited state? Even if relaxation dispersion can be unambiguously detected for a specific site in a biomolecule, initially it is often unknown what the dynamical process in question is. In other words, it is necessary to "assign" the excited state unambiguously.

If $\Delta\omega$ can be successfully derived in terms of both sign and magnitude, the chemical shift of the excited state may provide hints about its structural nature. A combination of relaxation dispersion with chemical shift-based methods such as CS-ROSETTA is particularly useful in this case [83]. Alternatively, the excited state chemical shift determined from $\Delta\omega$ may be compared with database reference chemical shifts from known structures or chemical shifts calculated by density functional theory [11]. Although the millisecond timescale exceeds the computational cost of most current laboratories for direct visualization of the dynamics by molecular dynamics (MD) simulations, visualization of possible dynamical processes by steered MD simulations is a potential computationally inexpensive approach [11]. In addition, comparison of the experimental relaxation dispersion-derived kinetic–thermodynamic data obtained from relaxation dispersion profiles acquired at different temperatures with theoretical free-energy calculations seems to be a successful strategy [11]. Lastly, it has been demonstrated that including additional biophysical methods such as single-molecule Förster resonance energy transfer (FRET), time-resolved X-ray crystallography, and principle component analysis (PCA) of conventional MD trajectories can successfully establish dynamical models of protein function over a wide range of timescales [84].

References

1. Sugase, K., Dyson, H.J., Wright, P.E.: Mechanism of coupled folding and binding of an intrinsically disordered protein. Nature **447**, 1021–1025 (2007)
2. Sugase, K., Lansing, J.C., Dyson, H.J., Wright, P.E.: Tailoring relaxation dispersion experiments for fast-associating protein complexes. J. Am. Chem. Soc. **129**, 13406–13407 (2007)
3. Boehr, D.D., McElheny, D., Dyson, H.J., Wright, P.E.: The dynamic energy landscape of dihydrofolate reductase catalysis. Science **313**, 1638–1642 (2006)
4. Henzler-Wildman, K.A., Thai, V., Lei, M., Ott, M., Wolf-Watz, M., Fenn, T., Pozharski, E., Wilson, M.A., Petsko, G.A., Karplus, M., Hübner, C.G., Kern, D.: Intrinsic motions along an enzymatic reaction trajectory. Nature **450**, 838–844 (2007)
5. Eisenmesser, E.Z., Millet, O., Labeikovsky, W., Korzhnev, D.M., Wolf-Watz, M., Bosco, D. A., Skalicky, J.J., Kay, L.E., Kern, D.: Intrinsic dynamics of an enzyme underlies catalysis. Nature **438**, 117–121 (2005)
6. Whittier, S.K., Hengge, A.C., Loria, J.P.: Conformational motions regulate phosphoryl transfer in related protein tyrosine phosphatases. Science **341**, 899–903 (2013)
7. Bhabha, G., Lee, J., Ekiert, D.C., Gam, J., Wilson, I.A., Dyson, H.J., Benkovic, S.J., Wright, P.E.: A Dynamic knockout reveals that conformational fluctuations influence the chemical step of enzyme catalysis. Science **332**, 234–238 (2011)

8. Harada, E., Sugishima, M., Harada, J., Fukuyama, K., Sugase, K.: Distal regulation of heme binding of heme oxygenase-1 mediated by conformational fluctuations. Biochemistry **54**, 340–348 (2015)
9. Sprangers, R., Gribun, A., Hwang, P.M., Houry, W.A., Kay, L.E.: Quantitative NMR spectroscopy of supramolecular complexes: dynamic side pores in ClpP are important for product release. Proc. Natl. Acad. Sci. U S A **102**, 315–320 (2005)
10. Kimsey, I.J., Petzold, K., Sathyamoorthy, B., Stein, Z.W., Al-Hashimi, H.M.: Visualizing transient Watson–Crick-like mispairs in DNA and RNA duplexes. Nature **519**, 315–320 (2015)
11. Nikolova, E.N., Kim, E., Wise, A.A., O'Brien, P.J., Andricioaei, I., Al-Hashimi, H.M.: Transient Hoogsteen base pairs in canonical duplex DNA. Nature **470**, 498–502 (2011)
12. Morimoto, D., Walinda, E., Fukada, H., Sugase, K., Shirakawa, M.: Ubiquitylation directly induces fold destabilization of proteins. Sci. Rep. **6**, 1–9 (2016)
13. Meinhold, D.W., Wright, P.E.: Measurement of protein unfolding/refolding kinetics and structural characterization of hidden intermediates by NMR relaxation dispersion. Proc. Natl. Acad. Sci. U S A **108**, 9078–9083 (2011)
14. Yanagi, K., Sakurai, K., Yoshimura, Y., Konuma, T., Lee, Y.-H., Sugase, K., Ikegami, T., Naiki, H., Goto, Y.: The monomer–seed interaction mechanism in the formation of the β2-microglobulin amyloid fibril clarified by solution NMR techniques. J. Mol. Biol. **422**, 390–402 (2012)
15. Neudecker, P., Robustelli, P., Cavalli, A., Walsh, P., Lundstrom, P., Zarrine-Afsar, A., Sharpe, S., Vendruscolo, M., Kay, L.E.: Structure of an intermediate state in protein folding and aggregation. Science **336**, 362–366 (2012)
16. Arai, M., Sugase, K., Dyson, H.J., Wright, P.E.: Conformational propensities of intrinsically disordered proteins influence the mechanism of binding and folding. Proc. Natl. Acad. Sci. U S A **112**, 9614–9619 (2015)
17. Schneider, R., Maurin, D., Communie, G., Kragelj, J., Hansen, D.F., Ruigrok, R.W., Jensen, M.R., Blackledge, M.: Visualizing the molecular recognition trajectory of an intrinsically disordered protein using multinuclear relaxation dispersion NMR. J. Am. Chem. Soc. **137**, 1220–1229 (2015)
18. Tzeng, S.R., Kalodimos, C.G.: Dynamic activation of an allosteric regulatory protein. Nature **462**, 368–372 (2009)
19. Carr, H.Y., Purcell, E.M.: Effects of diffusion on free precession in nuclear magnetic resonance experiments. Phys. Rev. **94**, 630–638 (1954)
20. Loria, J.P., Rance, M., Palmer, A.G.: A relaxation-compensated Carr–Purcell–Meiboom–Gill sequence for characterizing chemical exchange by NMR spectroscopy. J. Am. Chem. Soc. **121**, 2331–2332 (1999)
21. Meiboom, S., Gill, D.: Modified spin-echo method for measuring nuclear relaxation times. Rev. Sci. Instrum. **29**, 688–691 (1958)
22. Hansen, A.L., Nikolova, E.N., Casiano-Negroni, A., Al-Hashimi, H.M.: Extending the range of microsecond-to-millisecond chemical exchange detected in labeled and unlabeled nucleic acids by selective carbon $R_{1\rho}$ NMR spectroscopy. J. Am. Chem. Soc. **131**, 3818–3819 (2009)
23. Hansen, D.F., Vallurupalli, P., Kay, L.E.: Using relaxation dispersion NMR spectroscopy to determine structures of excited, invisible protein states. J. Biomol. NMR **41**, 113–120 (2008)
24. Walinda, E., Morimoto, D., Nishizawa, M., Shirakawa, M., Sugase, K.: Efficient identification and analysis of chemical exchange in biomolecules by $R_{1\rho}$ relaxation dispersion with *Amaterasu*. Bioinformatics **32**, 2539–2541 (2016)
25. Korzhnev, D.M., Orekhov, V.Y., Kay, L.E.: Off-resonance $R_{1\rho}$ NMR studies of exchange dynamics in proteins with low spin-lock fields: an application to a Fyn SH3 domain. J. Am. Chem. Soc. **127**, 713–721 (2005)
26. Miloushev, V.Z., Palmer, A.G.: $R_{1\rho}$ relaxation for two-site chemical exchange: general approximations and some exact solutions. J. Magn. Reson. **177**, 221–227 (2005)

27. Massi, F., Grey, M.J., Palmer, A.G.: Microsecond timescale backbone conformational dynamics in ubiquitin studied with NMR $R_{1\rho}$ relaxation experiments. Protein Sci. **14**, 735–742 (2005)
28. Massi, F., Johnson, E., Wang, C., Rance, M., Palmer, A.G.: NMR $R_{1\rho}$ rotating-frame relaxation with weak radio frequency fields. J. Am. Chem. Soc. **126**, 2247–2256 (2004)
29. Palmer, A.G., Kroenke, C.C., Loria, J.P.: Nuclear magnetic resonance methods for quantifying microsecond-to-millisecond motions in biological macromolecules. Methods Enzymol. **339**, 204–238 (2001)
30. Bothe, J.R., Nikolova, E.N., Eichhorn, C.D., Chugh, J., Hansen, A.L., Al-Hashimi, H.M.: Characterizing RNA dynamics at atomic resolution using solution-state NMR spectroscopy. Nat. Methods **8**, 919–931 (2011)
31. Furukawa, A., Konuma, T., Yanaka, S., Sugase, K.: Quantitative analysis of protein–ligand interactions by NMR. Prog. Nucl. Magn. Reson. Spectrosc. **96**, 47–57 (2016)
32. Loria, J.P., Rance, M., Palmer, A.G.: A TROSY CPMG sequence for characterizing chemical exchange in large proteins. J. Biomol. NMR **15**, 151–155 (1999)
33. Tollinger, M., Skrynnikov, N.R., Mulder, F.A., Forman-Kay, J.D., Kay, L.E.: Slow dynamics in folded and unfolded states of an SH3 domain. J. Am. Chem. Soc. **123**, 11341–11352 (2001)
34. Skrynnikov, N.R., Mulder, F.A., Hon, B., Dahlquist, F.W., Kay, L.E.: Probing slow time scale dynamics at methyl-containing side chains in proteins by relaxation dispersion NMR measurements: application to methionine residues in a cavity mutant of T4 lysozyme. J. Am. Chem. Soc. **123**, 4556–4566 (2001)
35. Ishima, R., Torchia, D.A.: Extending the range of amide proton relaxation dispersion experiments in proteins using a constant-time relaxation-compensated CPMG approach. J. Biomol. NMR **25**, 243–348 (2003)
36. Orekhov, V.Y., Korzhnev, D.M., Kay, L.E.: Double-and zero-quantum NMR relaxation dispersion experiments sampling millisecond time scale dynamics in proteins. J. Am. Chem. Soc. **126**, 1886–1891 (2004)
37. Guenneugues, M., Berthault, P., Desvaux, H.: A method for determining B_1 field inhomogeneity: are the biases assumed in heteronuclear relaxation experiments usually underestimated? J. Magn. Reson. **136**, 118–126 (1999)
38. Ban, D., Gossert, A.D., Giller, K., Becker, S., Griesinger, C., Lee, D.: Exceeding the limit of dynamics studies on biomolecules using high spin-lock field strengths with a cryogenically cooled probehead. J. Magn. Reson. **221**, 1–4 (2012)
39. Szyperski, T., Luginbühl, P., Otting, G., Güntert, P., Wüthrich, K.: Protein dynamics studied by rotating frame ^{15}N spin relaxation times. J. Biomol. NMR **3**, 151–164 (1993)
40. Mulder, F.A., de Graaf, R.A., Kaptein, R., Boelens, R.: An off-resonance rotating frame relaxation experiment for the investigation of macromolecular dynamics using adiabatic rotations. J. Magn. Reson. **131**, 351–357 (1998)
41. Zinn-Justin, S., Berthault, P., Guenneugues, M., Desvaux, H.: Off-resonance RF fields in heteronuclear NMR: application to the study of slow motions. J. Biomol. NMR **10**, 363–372 (1997)
42. Akke, M., Palmer, A.G.: Monitoring macromolecular motions on microsecond to millisecond time scales by $R_{1\rho}$–R_1 constant relaxation time NMR spectroscopy. J. Am. Chem. Soc. **118**, 911–912 (1996)
43. Cavanagh, J., Fairbrother, W.J., Palmer, A.G., Skelton, N.J.: Protein NMR Spectroscopy: Principles and Practice. Academic Press, New York (1996)
44. Walinda, E., Morimoto, D., Shirakawa, M., Sugase, K.: Practical considerations for investigation of protein conformational dynamics by ^{15}N $R_{1\rho}$ relaxation dispersion. J. Biomol. NMR **67**, 201–209 (2017)
45. Hartmann, S., Hahn, E.: Nuclear double resonance in the rotating frame. Phys. Rev. **128**, 2042–2053 (1962)
46. Pelupessy, P., Chiarparin, E.: Hartmann–Hahn polarization transfer in liquids: an ideal tool for selective experiments. Concepts Magn. Reson. **12**, 103–124 (2000)

47. Bak, M., Rasmussen, J.T., Nielsen, N.C.: SIMPSON: a general simulation program for solid-state NMR spectroscopy. J. Magn. Reson. **213**, 366–400 (2011)
48. Helmus, J.J., Jaroniec, C.P.: Nmrglue: an open source Python package for the analysis of multidimensional NMR data. J. Biomol. NMR **55**, 355–367 (2013)
49. Chen, L., Weng, Z., Goh, L., Garland, M.: An efficient algorithm for automatic phase correction of NMR spectra based on entropy minimization. J. Magn. Reson. **158**, 164–168 (2002)
50. Sugase, K., Konuma, T., Lansing, J.C., Wright, P.E.: Fast and accurate fitting of relaxation dispersion data using the flexible software package GLOVE. J. Biomol. NMR **56**, 275–283 (2013)
51. Vallurupalli, P., Hansen, D.F., Kay, L.E.: Structures of invisible, excited protein states by relaxation dispersion NMR spectroscopy. Proc. Natl. Acad. Sci. U S A **105**, 11766–11771 (2008)
52. Jiang, B., Yu, B., Zhang, X., Liu, M., Yang, D.: A ^{15}N CPMG relaxation dispersion experiment more resistant to resonance offset and pulse imperfection. J. Magn. Reson. **257**, 1–7 (2015)
53. LaPlante, S.R., Aubry, N., Déziel, R., Ni, F., Xu, P.: Transferred ^{13}C T_1 relaxation at natural isotopic abundance: a practical method for determining site-specific changes in ligand flexibility upon binding to a macromolecule. J. Am. Chem. Soc. **122**, 12530–12535 (2000)
54. Su, X.-C., Jergic, S., Ozawa, K., Burns, N.D., Dixon, N.E., Otting, G.: Measurement of dissociation constants of high-molecular weight protein–protein complexes by transferred ^{15}N-relaxation. J. Biomol. NMR **38**, 65–72 (2007)
55. Williamson, M.P.: Using chemical shift perturbation to characterise ligand binding. Prog. Nucl. Magn. Reson. Spectrosc. **73**, 1–16 (2013)
56. Walinda, E., Morimoto, D., Sugase, K., Konuma, T., Tochio, H., Shirakawa, M.: Solution structure of the ubiquitin-associated (UBA) domain of human autophagy receptor NBR1 and its interaction with ubiquitin and polyubiquitin. J. Biol. Chem. **289**, 13890–13902 (2014)
57. Hansen, D.F., Vallurupalli, P., Kay, L.E.: An improved ^{15}N relaxation dispersion experiment for the measurement of millisecond time-scale dynamics in proteins. J. Phys. Chem. B **112**, 5898–5904 (2008)
58. Vallurupalli, P., Hansen, D.F., Stollar, E., Meirovitch, E., Kay, L.E.: Measurement of bond vector orientations in invisible excited states of proteins. Proc. Natl. Acad. Sci. U S A **104**, 18473–18477 (2007)
59. Farrow, N.A., Zhang, O., Forman-Kay, J.D., Kay, L.E.: A heteronuclear correlation experiment for simultaneous determination of ^{15}N longitudinal decay and chemical exchange rates of systems in slow equilibrium. J. Biomol. NMR **4**, 727–734 (1994)
60. Sahu, D., Clore, G.M., Iwahara, J.: TROSY-based z-exchange spectroscopy: application to the determination of the activation energy for intermolecular protein translocation between specific sites on different DNA molecules. J. Am. Chem. Soc. **129**, 13232–13237 (2007)
61. Li, Y., Palmer, A.G.: TROSY-selected ZZ-exchange experiment for characterizing slow chemical exchange in large proteins. J. Biomol. NMR **45**, 357–360 (2009)
62. Vallurupalli, P., Bouvignies, G., Kay, L.E.: Studying "invisible" excited protein states in slow exchange with a major state conformation. J. Am. Chem. Soc. **134**, 8148–8161 (2012)
63. Bouvignies, G., Kay, L.E.: A 2D ^{13}C-CEST experiment for studying slowly exchanging protein systems using methyl probes: an application to protein folding. J. Biomol. NMR **53**, 303–310 (2012)
64. Fawzi, N.L., Ying, J., Ghirlando, R., Torchia, D.A., Clore, G.M.: Atomic-resolution dynamics on the surface of amyloid-β protofibrils probed by solution NMR. Nature **480**, 268–272 (2011)
65. Demers, J.P., Mittermaier, A.: Binding mechanism of an SH3 domain studied by NMR and ITC. J. Am. Chem. Soc. **131**, 4355–4367 (2009)
66. McConnell, H.M.: Reaction rates by nuclear magnetic resonance. J. Chem. Phys. **28**, 430–431 (1958)

67. Korzhnev, D.M., Salvatella, X., Vendruscolo, M., Di Nardo, A.A., Davidson, A.R., Dobson, C.M., Kay, L.E.: Low-populated folding intermediates of Fyn SH3 characterized by relaxation dispersion NMR. Nature **430**, 586–590 (2004)
68. Carver, J.P., Richards, R.E.: A general two-site solution for the chemical exchange produced dependence of T_2 upon the Carr–Purcell pulse separation. J. Magn. Reson. **6**, 89–105 (1969)
69. Goto, N.K., Zor, T., Martinez-Yamout, M., Dyson, H.J., Wright, P.E.: Cooperativity in transcription factor binding to the coactivator CREB-binding protein (CBP). The mixed lineage leukemia protein (MLL) activation domain binds to an allosteric site on the KIX domain. J. Biol. Chem. **277**, 43168–43174 (2002)
70. Hwang, T.-L., van Zijl, P.C., Mori, S.: Accurate quantitation of water-amide proton exchange rates using the phase-modulated CLEAN chemical EXchange (CLEANEX-PM) approach with a Fast-HSQC (FHSQC) detection scheme. J. Biomol. NMR **11**, 221–226 (1998)
71. Li, Z., Scheraga, H.A.: Monte Carlo-minimization approach to the multiple-minima problem in protein folding. Proc. Natl. Acad. Sci. U S A **84**, 6611–6615 (1987)
72. Metropolis, N., Rosenbluth, A.W., Rosenbluth, M.N., Teller, A.H., Teller, E.: Equation of state calculations by fast computing machines. J. Chem. Phys. **21**, 1087–1092 (1953)
73. Kirkpatrick, S., Gelatt, C.D., Vecchi, M.P.: Optimization by simulated annealing. Science **220**, 671–680 (1983)
74. Matsuki, Y., Konuma, T., Fujiwara, T., Sugase, K.: Boosting protein dynamics studies using quantitative nonuniform sampling NMR spectroscopy. J. Phys. Chem. B **115**, 13740–13745 (2011)
75. Ishima, R., Torchia, D.A.: Error estimation and global fitting in transverse-relaxation dispersion experiments to determine chemical-exchange parameters. J. Biomol. NMR **32**, 41–54 (2005)
76. Press, W.H.: Numerical Recipes 3rd edition: The Art of Scientific Computing. Cambridge University Press, Cambridge (2007)
77. Mosteller, F., Tukey, J.W.: Data analysis, including statistics. Handbook of Social Psychology, pp. 80–203 (1968)
78. Schanda, P., Brutscher, B., Konrat, R., Tollinger, M.: Folding of the KIX domain: characterization of the equilibrium analog of a folding intermediate using $^{15}N/^{13}C$ relaxation dispersion and fast $^{1}H/^{2}H$ amide exchange NMR spectroscopy. J. Mol. Biol. **380**, 726–741 (2008)
79. Konuma, T., Harada, E., Sugase, K.: Extracting protein dynamics information from overlapped NMR signals using relaxation dispersion difference NMR spectroscopy. J. Biomol. NMR **63**, 367–373 (2015)
80. Korzhnev, D.M., Kloiber, K., Kanelis, V., Tugarinov, V., Kay, L.E.: Probing slow dynamics in high molecular weight proteins by methyl-TROSY NMR spectroscopy: application to a 723-residue enzyme. J. Am. Chem. Soc. **126**, 3964–3973 (2004)
81. Toyama, Y., Osawa, M., Yokogawa, M., Shimada, I.: NMR method for characterizing microsecond-to-millisecond chemical exchanges utilizing differential multiple-quantum relaxation in high molecular weight proteins. J. Am. Chem. Soc. **138**, 2302–2311 (2016)
82. Walinda, E., Morimoto, D., Shirakawa, M., Sugase, K.: F_1F_2-selective NMR spectroscopy. J. Biomol. NMR **68**, 41–52 (2017)
83. Lange, O.F., Rossi, P., Sgourakis, N.G., Song, Y., Lee, H.-W., Aramini, J.M., Ertekin, A., Xiao, R., Acton, T.B., Montelione, G.T., Baker, D.: Determination of solution structures of proteins up to 40 kDa using CS-Rosetta with sparse NMR data from deuterated samples. Proc. Natl. Acad. Sci. U S A **109**, 10873–10878 (2012)
84. Henzler-Wildman, K.A., Lei, M., Thai, V., Kerns, S.J., Karplus, M., Kern, D.: A hierarchy of timescales in protein dynamics is linked to enzyme catalysis. Nature **450**, 913–916 (2007)
85. Piotto, M., Saudek, V., Sklenář, V.: Gradient-tailored excitation for single-quantum NMR spectroscopy of aqueous solutions. J. Biomol. NMR **2**, 661–665 (1992)
86. Shaka, A., Keeler, J., Freeman, R.: Evaluation of a new broadband decoupling sequence: WALTZ-16. J. Magn. Reson. **53**, 313–340 (1969)

87. Davis, D., Perlman, M., London, R.: Direct measurements of the dissociation-rate constant for inhibitor-enzyme complexes via the $T_{1\rho}$ and T_2 (CPMG) methods. J. Magn. Reson. B **104**, 266–275 (1994)
88. Deverell, C., Morgan, R., Strange, J.: Studies of chemical exchange by nuclear magnetic relaxation in the rotating frame. Mol. Phys. **18**, 553–559 (1970)
89. Abergel, D., Palmer, A.G.: On the use of the stochastic Liouville equation in nuclear magnetic resonance: application to $R_{1\rho}$ relaxation in the presence of exchange. Concepts Magn. Reson. Part A **19**, 134–148 (2003)
90. Trott, O., Palmer, A.G.: $R_{1\rho}$ relaxation outside of the fast-exchange limit. J. Magn. Reson. **154**, 157–160 (2002)
91. Trott, O., Abergel, D., Palmer, A.G.: An average-magnetization analysis of $R_{1\rho}$ relaxation outside of the fast exchange limit. Mol. Phys. **101**, 753–763 (2003)
92. Koss, H., Rance, M., Palmer, A.G.: General expressions for $R_{1\rho}$ relaxation for *N*-site chemical exchange and the special case of linear chains. J. Magn. Reson. **274**, 36–45 (2017)
93. Luz, Z., Meiboom, S.: Nuclear magnetic resonance study of the protolysis of trimethylammonium ion in aqueous solution—order of the reaction with respect to solvent. J. Chem. Phys. **39**, 366–370 (1963)
94. Ishima, R., Torchia, D.A.: Estimating the time scale of chemical exchange of proteins from measurements of transverse relaxation rates in solution. J. Biomol. NMR **14**, 369–372 (1999)
95. Bloom, M., Reeves, L., Wells, E.: Spin echoes and chemical exchange. J. Chem. Phys. **43**, 1615–1624 (1965)